Biophysical Chemistry, 48 (1993) 205–220
Elsevier Science Publishers B.V., Amsterdam

BIOCHE 01810

Fluorescence decay of DPH in lipid membranes: influence of the external refractive index

D. Toptygin and L. Brand *

McCollum-Pratt Institute, The Department of Biology, The Johns Hopkins University, 34th and Charles Streets, Baltimore, MD 21218 (USA)

(Received 19 April 1993; accepted in revised form 30 August 1993)

Abstract

The radiative decay rate of a fluorescent probe in an optically thin layer is known to depend on the orientation of the probe and on the refractive indices inside and outside the layer (W. Lukosz, Phys. Rev. B 22 (1980) 3030). Fluorescent probes in phospholipid bilayer membranes approximate such a system. The natural lifetime is expected to vary with the refractive index of the medium surrounding the bilayer. The lifetime variation with the refractive index depends on the orientation of the fluorescent probe. This can be used to retrieve the second-rank orientational order parameter, $\langle P_2 \rangle$. The fluorescence decay of all-trans 1,6-diphenyl-1,3,5-hexatriene in L-α-dipalmitoyl-phosphatidylcholine large unilamellar vesicles (LUVs) was measured at a temperature well below that of the phase transition. The refractive index of the medium was varied by addition of glycerol or sucrose. The observed change of decay time with the refractive index followed the theoretical prediction. The value of the order parameter, $\langle P_2 \rangle$, recovered is significantly lower than that obtained from fluorescence polarization data. Possible reasons for this disagreement are discussed.

Keywords: Fluorescence; Natural lifetime; Refractive index; Lipid membranes; Orientational order; Diphenylhexatriene

1. Introduction

The fluorescence lifetime of a molecule can change due to several reasons. The fluorescence lifetime is the inverse of the sum of the radiative and non-radiative decay rates. The non-radiative rate depends on the rate of collisions between molecules and on the accessibility of certain quenchers, e.g. O_2, heavy atoms, etc. The radiative rate and its inverse, the natural lifetime, depends on the optical environment of the molecule. For example, the natural lifetime of a fluorescent probe in an ideal homogeneous isotropic medium depends on the refractive index of the medium. The natural lifetime in an inhomogeneous and/or anisotropic optical environment will depend on the location and/or orientation of the fluorescent probe.

The radiation of an electric dipole oscillator from inside an optically thin layer was considered by Lukosz [1]. It was shown, that the radiative decay rate depends on the refractive indices inside and outside the layer and on the angle, θ,

* Corresponding author.

between the dipole and the normal to the surface of the layer. A phospholipid bilayer membrane is a good example of an optically thin layer because its thickness usually does not exceed 1/8 of the light wavelength ($\lambda/8 \approx 50$ nm).

The orientational dependence of the radiative decay rate in bilayer membranes was investigated in our previous studies [2,3]. Experiments were carried out as a function of temperature both below and above the phase transition temperature. The radiative rate was changing as the probe rotated, therefore explicit assumptions had to be made regarding the rotational motion of the probe in order to predict the fluorescence decay. In addition, the refractive index of the bilayer interior was unknown. This refractive index and the parameters describing the rotational dynamics were floated as unknown fitting parameters in the global analysis of the fluorescence and polarization decay data [3].

The refractive index in the lipid bilayer can be measured directly, making use of the fact that the light scattering by vesicle suspensions reaches a minimum when the refractive index of the medium in which the vesicles were made best matches that of the bilayer interior. Changes in the light scattering with the refractive index of the medium have been observed experimentally [4,5].

Varying the refractive index of the medium offers a unique opportunity to measure the orientation of a fluorescent probe with respect to the bilayer. It has been shown, that the radiative rate for the dipole oriented along the normal ($\theta = 0°$) and along the surface ($\theta = 90°$) must change as the fifth and as the first power of the refractive index, respectively [1]. When the refractive index of the bilayer is known, the radiative rate for every intermediate orientation can be predicted theoretically. This can be used to evaluate the second-rank orientational order parameter, $\langle P_2(\cos\theta)\rangle$.

The second-rank order parameter in bilayer membranes is commonly evaluated from time-resolved fluorescence polarization data. The theory of fluorescence depolarization in membranes was originally developed in [6–11]; for a recent review, see [12]. It is of interest to compare the values of the order parameter obtained with the same fluorescent probe in the same bilayer by two different methods: fluorescence polarization and natural lifetime.

2. Theory

2.1. Refractive index

The efficiency of light scattering by lipid bilayers of refractive index n_1 immersed in a medium of refractive index n_0 depends on the difference between n_1 and n_0. When the refractive indices are matched, $n_0 = n_1$, the scattered intensity reaches a minimum. For a quantitative description of the scattering efficiency one can use either absorbance [4] or the intensity of scattered light [5]. In the latter case the absorbance of the sample should not exceed 0.02 to avoid inner-filter effects. In the vicinity of $n_0 = n_1$ the scattering efficiency can be described by the parabola

$$A = \alpha(n_0 - n_1)^2 + \beta, \tag{1}$$

where A is absorbance, α is a constant that depends on the wavelength, size, shape and concentration of the vesicles, and β stands for the minimum losses. If the refractive index in the lipid bilayer is perfectly homogeneous, β equals zero. The β term is introduced since inhomogeneity of the refractive index is expected for hydrated phospholipid bilayers. In this case n_1 is an average refractive index in the bilayer. The β term also contains a small contribution from the Rayleigh scatter, which is typically four or five orders of magnitude weaker than the light scattered by LUVs.

Eq. (1) can be obtained from the Taylor expansion of the function $A(n_0)$ in the vicinity of the minimum. The term containing the first power of $(n_0 - n_1)$ is absent in the expansion because the function has a minimum at $n_0 = n_1$. The terms of the third and higher powers of the refractive index can be neglected when the variation of n_0 is very small (it is experimentally impossible to obtain a large variation of the refractive index).

Absorbance estimates of scattering efficiency should be made on unlabelled vesicles and/or at a wavelength outside the absorption band of the fluorescent probe or the bilayer material. The refractive index of the entrapped medium should not differ significantly from that of the medium surrounding the vesicles. The refractive index of the bilayer can be evaluated by fitting the parabola given in eq. (1) to experimental data. Deviations from the parabola would be indicative of variations in the size or shape of the vesicles or in the lipid concentration.

2.2. Fluorescence decay

Fluorescence decay of a given fluorescent probe in a certain local environment and at a certain orientation is characterized by a single decay rate or its inverse the lifetime, τ. Further theoretical discussion will be restricted to fluorophores for which this is the case. The decay rate and the lifetime may change with the orientation and location of the probe. The decay rate is the sum of the rates of the radiative (k_r) and non-radiative (k_{nr}) processes:

$$\frac{1}{\tau} = k_r + k_{nr}. \tag{2}$$

If the probe has a high quantum yield, then the non-radiative rate will have little effect on its lifetime, and the changes in the lifetime will reflect the changes in the radiative rate. The radiative decay rate for a fluorescent probe in a thin layer is given by the following equation (the thickness of the layer must be less than 1/8 of the light wavelength):

$$k_r = \frac{4\omega^3}{3\hbar c^3} f^2 |\mu|^2 n_0 \times \left(\sin^2\theta + \frac{n_0^4}{n_1^4} \cos^2\theta \right), \tag{3}$$

where ω is the circular frequency of fluorescence light, $\hbar$ is Planck's constant, c is the speed of light, f is the factor that accounts for the difference between the local electric field experienced by the probe and the macroscopic field inside the layer, μ is the matrix element of the electric dipole operator (emission dipole), n_1 and n_0 are the refractive indices of the layer and the surrounding medium, and θ is the angle between the emission dipole and the normal to the surface of the layer. The explicit derivation of eq. (3) can be found in Appendix A. Lukosz [1] obtained a result similar to eq. (3) for the radiation of a classical dipole in a thin layer. Eq. (3) is derived for a quantum object, i.e. a fluorescent molecule.

The radiative rate depends on the orientation of the probe with respect to the membrane bilayer and can thus be used to measure the orientation of the probe. If all the constants involved in eq. (3) were known, it would be possible to calculate the angle θ from the experimental values of the lifetime and the quantum yield. Unfortunately, state-of-the-art quantum-mechanical calculations of the emission dipoles for polyatomic molecules are at best approximate, while the precise calculation of the factor f would in addition require knowledge of the coordinates and polarizability of every electron in the near environment of the fluorescent probe. These circumstances make it impossible to determine the orientation of the probe from a single pair of lifetime and quantum yield measurements.

Assume that the refractive index outside the membrane bilayer can be varied without significantly disturbing the physical properties of the bilayer (the validity of this assumption is analyzed in the discussion section). The effect of the refractive index on the decay rate will be different for different orientations of the probe. For instance, if a rod-like probe having its emission dipole parallel to the rod axis is aligned along the normal to the surface of the membrane bilayer, $\theta = 0$, then k_r must change proportionally to the fifth power of n_0. If the same probe is aligned parallel to the surface of the bilayer, $\theta = 90°$, then k_r will change as the first power of n_0. In the case of intermediate orientations the dependence is represented by the following polynomial:

$$k_r = \left(\tfrac{3}{2}\gamma \sin^2\theta\right) n_0 + \left(\tfrac{3}{2}\gamma n_1^{-4} \cos^2\theta\right) n_0^5, \tag{4}$$

where $\frac{3}{2}\gamma$ is the combination of several constants from eq. (3).

It is known, that a fluorescent probe may have a distribution of orientations in the membrane bilayer. For the monodomain case, either a single lifetime or a continuous distribution of lifetimes will be observed depending on the relation between the rotational relaxation time and the fluorescence decay time [2]. In the case where rotation is much faster than decay, the fluorescence of each probe molecule will decay with the mean rate, which can be obtained by averaging the rate from eq. (4) over the orientational distribution of the probe,

$$\begin{aligned}\langle k_r\rangle &= \tfrac{3}{2}\gamma\langle\sin^2\theta\rangle n_0 + \tfrac{3}{2}\gamma n_1^{-4}\langle\cos^2\theta\rangle n_0^5 \\ &= \gamma(1-\langle P_2\rangle)n_0 + \gamma n_1^{-4}(\langle P_2\rangle + \tfrac{1}{2})n_0^5,\end{aligned} \tag{5}$$

where $\langle P_2\rangle = \langle(3\cos^2\theta - 1)/2\rangle$. The expression for the lifetime can then be obtained by substituting the mean k_r from eq. (5) in eq. (2),

$$\begin{aligned}\frac{1}{\tau} &= k_{nr} + \gamma(1-\langle P_2\rangle)n_0 \\ &\quad + \gamma n_1^{-4}(\langle P_2\rangle + \tfrac{1}{2})n_0^5.\end{aligned} \tag{6}$$

In the case, where the probe rotation is much slower than the decay, every probe molecule will have an individual decay time, therefore, one should observe a continuous distribution of lifetimes. The longest and the shortest lifetime in all cases cannot differ by more than a factor of $(n_1/n_0)^4$ or even less, if the contribution of the non-radiative rate is significant. The ability to experimentally distinguish a distribution of lifetimes from a single lifetime depends mainly on the width of the distribution. If the longest and the shortest lifetime in the distribution differ by less than a factor of two, it is very difficult to distinguish a distribution from a single lifetime. For example, in the case of continuously variable frequency phase and modulation data, the difference between a uniform distribution of lifetimes with $\tau_{max}/\tau_{min} = 1.8$ and a single lifetime does not exceed 0.5° by phase and 0.009 by modulation (peak deviations). The root-mean-square deviations in this case do not exceed 0.15° by phase and 0.002 by modulation. In the case of a Gaussian or Lorentzian distribution with chopped-off tails, the deviations are substantially lower. The reported figures were obtained by numerical simulations.

When the distribution of lifetimes cannot be resolved, the mean lifetime in the distribution can still be measured. The mean lifetime can be expressed as follows:

$$\begin{aligned}\bar{\tau} &= \int_0^\infty tI(t)\,dt \Big/ \int_0^\infty I(t)\,dt \\ &= \frac{\int_0^\pi k_r(\theta)\left[k_r(\theta)+k_{nr}\right]^{-2}\xi(\theta)P(\theta)\sin\theta\,d\theta}{\int_0^\pi k_r(\theta)\left[k_r(\theta)+k_{nr}\right]^{-1}\xi(\theta)P(\theta)\sin\theta\,d\theta},\end{aligned} \tag{7}$$

where $k_r(\theta)$ can be taken from eq. (4), $\xi(\theta)$ is the orientational dependence of the probability of excitation, which has been shown to be proportional to $k_r(\theta)$ [2,3], and $P(\theta)$ is the orientational distribution of the fluorescent probe molecule. After a series of transformations the inverse of this mean lifetime can be represented in the following way:

$$\begin{aligned}1/\bar{\tau} &= k_{nr} + \gamma(1-\langle P_2\rangle)n_0 \\ &\quad + \gamma n_1^{-4}(\langle P_2\rangle + \tfrac{1}{2})n_0^5 \\ &\quad + \frac{\int_0^\pi \dfrac{k_r(\theta)P(\theta)\sin\theta\,d\theta}{\left[1+k_{nr}/k_r(\theta)\right]^2}}{\int_0^\pi \dfrac{P(\theta)\sin\theta\,d\theta}{\left[1+k_{nr}/k_r(\theta)\right]^2}} \\ &\quad - \frac{\int_0^\pi k_r(\theta)P(\theta)\sin\theta\,d\theta}{\int_0^\pi P(\theta)\sin\theta\,d\theta}.\end{aligned} \tag{8}$$

If $k_{nr} = 0$ or $n_0 = n_1$, then the difference between the two ratios of integrals in eq. (8) equals zero. Only if the quantum yield is not high, and the difference between the refractive indices is large, the difference between the two ratios may give a significant contribution. The contribution of this difference was calculated numerically for various

values of quantum yield in the range from 0 to 100%, various ratios of n_0/n_1, in the range from 0.90 to 1.10, and various orientational distributions $P(\theta)$ covering the range from $\langle P_2 \rangle = -0.5$ to $+1.0$. The largest contribution of the difference between the two ratios on the right-hand side of eq. (8) did not exceed 0.89%. This is the maximum error that can be introduced by neglecting the two ratios of integrals. The error is proportional to the second power of $(n_0 - n_1)$. If the difference between the refractive indices does not exceed 7%, then the error will be less than 0.43%. If in addition if $\eta > 80\%$, then the error will drop below 0.27%. Such an error is not critical in the analysis of experimental data. When the small term in eq. (8) is dropped, it becomes identical to eq. (6), derived for the case of fast rotation.

In summary, if the difference between n_1 and n_0 does not exceed 10%, the decay will appear mono-exponential and eq. (6) will be valid to a good approximation independent of the relationship between the rotational rate and the decay rate. This equation can be used to fit experimental data, and in principle it can be used to determine the order parameter $\langle P_2 \rangle$. In practice, however, not all of the parameters involved in eq. (6) can be determined from fitting lifetime data. If the refractive index n_0 can be varied only within a few percent, the lifetime dependence will appear practically linear. From a linear dependence, only two parameters can be extracted, whereas eq. (6) contains four. At least two of these four parameters must therefore be measured in independent experiments. The value of n_1 can be measured as described above (see section 2.1). The following section describes a method of estimating k_{nr}.

2.3. Quantum yield

The non-radiative rate can be calculated from the values of lifetime, τ, and quantum yield, η,

$$k_{nr} = \frac{1 - \eta}{\tau}. \tag{9}$$

Measurement of the quantum yield of fluorescent probes in membranes is complicated by the fact that one cannot easily separate the losses in the excitation light due to absorption by the probe from those due to scattering. If the sample and the reference have identical absorbance, then the number of photons absorbed by the probe, N_a plus the number of photons scattered in the sample, N_s, equals the number of photons extracted from the excitation beam by the reference, N_r. The emission spectra obtained with the sample and with the reference must be corrected for the instrumental response and integrated. If the reference has a quantum yield of 1, the integral over the corrected reference spectrum yields N_r. In the emission spectrum, the scattering peak and fluorescence emission are separated, therefore integration of the corrected sample spectrum can be performed individually over the scattering peak and over the fluorescence spectrum. Since the quantum yield of scattering is one, the integral over the scattering peak must yield N_s. The integral over the fluorescence spectrum yields the number of emitted photons, N_e. The quantum yield of fluorescence is defined as N_e/N_a, where N_a can be evaluated only by subtracting N_s from N_r,

$$\eta = \frac{N_e}{N_r - N_s}. \tag{10}$$

This method of measuring the quantum yield in membranes assumes that the intensity of scattering in different directions is the same and that the sensitivity of the fluorometer to the scattered light and partially depolarized fluorescence light is the same. These assumptions hold true when the scattering particles are small compared to the light wavelength and the polarizers in the excitation and emission channels have the magic angle configuration.

2.4. Order parameter

With measured estimates of n_1 and k_{nr} available, the function given by eq. (6) can be fit to the lifetime data obtained in solutions of variable refractive index. In this fitting procedure the values of n_1 and k_{nr} must be fixed, or the measured dependence of k_{nr} on n_0 (if any) included,

whereas the values of γ and $\langle P_2 \rangle$ play the role of fitting parameters in a nonlinear least-squares analysis program. A graphical procedure can be also used to recover the value of $\langle P_2 \rangle$. The procedure is based on the fact that eq. (6) can be linearized in the following way:

$$y = Ax + B,$$

$$x = n_0^4,$$

$$y = \left(\frac{1}{\tau} - k_{nr} \right) / n_0. \tag{11}$$

Coefficients A and B can be determined by linear regression and the order parameter can be calculated according to eq. (12),

$$\langle P_2(\cos\theta) \rangle = \frac{An_1^4 - \frac{1}{2}B}{An_1^4 + B}. \tag{12}$$

In the proposed analysis of the lifetime dependence on the refractive index it was assumed that the values of the parameters γ, n_1, k_{nr}, and $\langle P_2 \rangle$ do not change when the refractive index of the medium surrounding the bilayers is varied. As the values of these parameters depend on the physical properties of the bilayer interior, they should not directly depend on the chemical composition of the surrounding medium unless the changes in this medium have some effect on the properties of the membrane bilayer.

3. Materials and methods

3.1. Preparation of vesicles

Vesicles were made of L-α-dipalmitoyl-phosphatidylcholine (DPPC) doped with 1,6-diphenyl-1,3,5-hexatriene (DPH). Both DPH and DPPC were the highest quality available from Sigma (crystalline). DPH and DPPC were dissolved in chloroform (Baker Analyzed Grade, which was tested for fluorescence and no appreciable emission was found). The mole fraction of DPH in DPPC was 1.0×10^{-3}. The solution was dried in thin films under nitrogen for at least 12 h. Dry films were hydrated in aqueous solutions of various refractive indices. In the preparation of unlabelled vesicles DPPC powder was hydrated directly. The suspension was extruded using the 10 ml thermobarrel extruder from Lipex Biomembranes Inc., Vancouver, British Columbia. The protocol described in [13] was followed to obtain 100 nm diameter large unilamellar vesicles (LUV_{100}s). For fluorescence measurements vesicles were diluted to a final lipid concentration of 0.9×10^{-4} M.

The refractive index of the solutions used in the vesicle preparation was varied by addition of either glycerol (up to 800 g/l) or sucrose (up to 600 g/l). Higher concentrations would dramatically increase the viscosity, which impairs the application of the extrusion technique. All solutions contained 150 mM NaCl and 20 mM Sodium-Phosphate buffer, pH = 7.6. Glycerol (anhydrous), sucrose (crystalline), and all other reagents used in the preparation of the solutions were "Baker Analyzed Grade". Solutions were tested for fluorescence. The solution containing the highest concentration of sucrose had a background fluorescence level not exceeding 1.5% of the DPH fluorescence intensity in the sample of standard concentration. The solutions containing only water and glycerol had background fluorescence intensity of less than 0.1%. The refractive indices were interpolated from the data in [14]. The effect of small quantities of sodium chloride and phosphate on the refractive index was neglected. The difference between the refractive index at the wavelength of the sodium D line and the wavelength of DPH fluorescence (α 0.01) was neglected.

Of the chemicals not related to vesicle preparation, paraffin oil was from VWR Scientific, San Francisco California (Saybolt viscosity 80-90 at 100°F), n-hexane was from Aldrich (Spectrophotometric Grade), cyclohexane was from Eastman Kodak, (Spectro ACS grade), 9,10-diphenylanthracene (DPA) was from Aldrich (99 + %), POPOP was from SIGMA, and absolute ethanol was from Warner-Graham Co, Cockeysville, Maryland.

3.2. Optical measurements

Absorbance was measured on an LKB 4050 single-beam spectrophotometer (LKB Biochrom,

Cambridge, England). The reproducibility of the measurements was ±0.001 absorbance units. All fluorescence measurements were carried out on the SLM-48000 multifrequency phase-and-modulation spectrofluorometer (SLM Instruments Inc., Urbana, Illinois). In dynamic fluorescence measurements the 365 nm Hg line was used for excitation. The light from a 200 W Hg–Xe arc lamp (Spectral Energy Corp., Westwood, New Jersey) was passed through a combination of Corning 7-60 and 0-52 filters to select the single spectral line. Emission was filtered by the short-cut filter KV-399 (cutoff wavelength 400 nm, transmission at 365 nm less than 0.1%. A magic angle configuration of polarizers excluded artifacts associated with dynamic depolarization. The choice of the excitation wavelength close to the peak of absorption of DPH substantially improved the spectral purity of the fluorescence signal. After a modification of the light modulator module (two collimating lenses and two diaphragms were introduced), the modulation ratio approximately doubled, which substantially improved the accuracy of the results. The random errors at most frequencies were less than 0.1° for phase and 0.001 for modulation. The error estimates were calculated from the statistics of the data itself. For this purpose every measurement was repeated 10 times. The errors were different at different frequencies. In the data analysis we used the errors individually calculated for every frequency and every sample. A fluorescence standard (POPOP solution in ethanol, $\tau = 1.295 \pm 0.005$ ns) was employed as a reference in order to avoid systematic errors due to color effects.

For the quantum yield measurements, the excitation wavelength chosen was 380 nm so as to improve the fluorescence/scattering ratio (scattering is inversely proportional to about the fourth power of the wavelength). The excitation light from a 450 W arc lamp was filtered by the monochromator (1 nm bandpass). The bandpass of the emission monochromator (4 nm) and the orientation of the polarizer in the emission channel (vertical) were set up to be the same as in the conditions for which the correction factors were obtained. The excitation polarizer was set up with its transmission vector at 55° to the vertical to give a magic angle condition. Three different references were employed: Ludox (colloid silica), unlabelled DPPC vesicles and a solution of DPA in cyclohexane (deoxygenated). The quantum yield of the scattering references was assumed to be 1.00. The quantum yield of DPA was also taken as unity [15]. To avoid unequal efficiency of light collection, the refractive index of the reference was matched with that of the sample (when possible). Inner filter effect was avoided by using dilute samples.

4. Results

4.1. Refractive index

Fig. 1 shows the absorbance of LUV_{100} suspensions prepared in solutions of different refractive indices. These data were obtained with unlabelled vesicles, but labelled vesicles have the same optical density at $\lambda = 450$ nm. The optical density data were fit by the parabola of eq. (1). The vertex of this parabola gave an estimate for the refractive index in the bilayer as $n_1 = 1.425$. This value falls in the range of refractive indices of saturated hydrocarbons (decane = 1.410, dode-

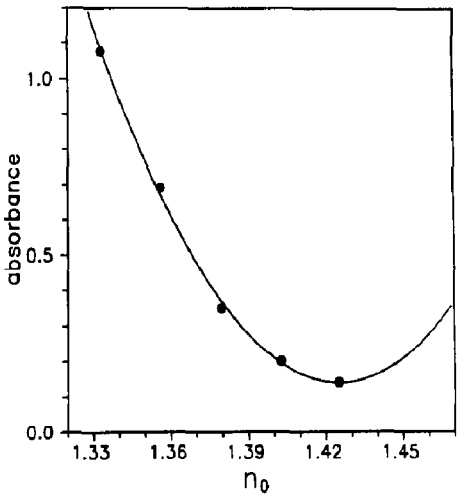

Fig. 1. Absorbance of LUV_{100} suspensions made in glycerol solutions of different refractive indices, n_0. Circles: experimental data. Curve: eq. (1). Experimental parameters: $\lambda = 450$ nm, DPPC concentration 5.0 ± 0.5 mg/ml, temperature 20 ± 2°C.

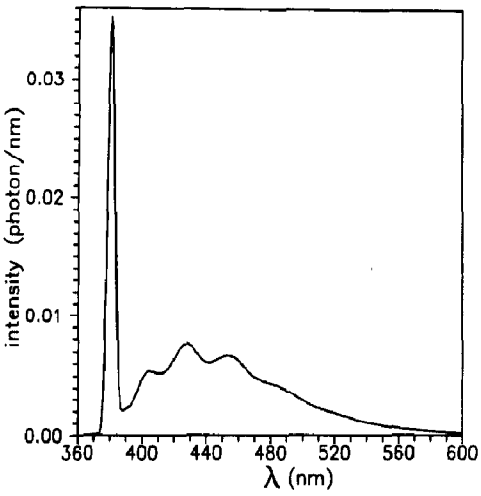

Fig. 2. Corrected spectral emission from the suspension of DPH-labelled DPPC LUV_{100}s made in the glycerol solution of the refractive index, $n_0 = 1.425$ and excited at $\lambda = 380$ nm. Integrating under this spectrum yielded the quantum yield, $\eta = 0.88$.

cane = 1.422, tetradecane = 1.429, hexadecane = 1.434, octadecane = 1.439). Since deviations of the experimental points from the parabola shown in Fig. 1 do not have a systematic character, therefore we have no indication that the size or shape of the vesicles was changing, although it should be pointed out that, because of the restriction on solvent viscosity imposed by the protocol for vesicle preparation, all the experimental points fall on one side of the parabola.

4.2. Fluorescence quantum yield

The attempts to measure the quantum yield of DPH in vesicles made in solutions of low refractive indices failed because of their very high scatter component, which resulted in erratic estimates of the denominator of eq. (8). The situation improved radically when solutions of refractive index close to $n_0 = 1.425$ were employed. The emission spectrum obtained for the solution having $n_0 = 1.425$ is shown in Fig. 2. The integral over the scattering peak in this case contributed less than a quarter of the total number of photons. The value of the quantum yield calculated from eq. (10) was 0.88 at 20°C. This value was obtained with use of scattering references and reproduced within ±2%. The yield obtained with the use of the fluorescent reference standard DPA was substantially higher, which can be explained if its quantum yield were lower than 1.00. The latter value was taken from [15], where several arguments for employing DPA as a fluorescent standard of unit quantum yield are presented.

The quantum yield of DPH reduces to ≈0.60 above the phase transition of DPPC, and keeps rapidly decreasing with temperature. Deoxygenation of the sample has only a marginal effect on the quantum yield of DPH in the membrane bilayers and in paraffin oil, where it is about 0.75 at 20°C. In contrast to these highly viscous environments, the quantum yield of DPH in light solvents strongly depends on the concentration of oxygen. In *n*-hexane, the quantum yield decreases from 0.76 in the absence of O_2 to 0.31 in equilibrium with atmospheric air (20°C).

4.3. Fluorescence lifetime

The phase and modulation data obtained at 20 ± 0.2°C with DPH labelled DPPC vesicles prepared in solutions of different refractive indices were fit to the models of one, two, three, and four discrete lifetimes. It was found that in all cases the model of three lifetimes was sufficient to fit the data. Adding a fourth lifetime produced no decrease in the χ^2 goodness of fit parameter, whereas decreasing the number of lifetimes to two and one produced approximately 10- and 200-fold increases in the χ^2. A typical fit between the experimental data and the models of two and three lifetimes is shown in Fig. 3. As a control the decay of a 2×10^{-6} M solution of DPH in paraffin oil was measured. The decay was found to be monoexponential, $\tau = 9.7 \pm 0.1$ ns at 20°C.

The values of the lifetimes and fractional intensities obtained for DPH in vesicles are shown in Table 1. The long lifetime component contributes more than 90% of the fluorescence intensity. If the DPH probe had a high orientational order in the bilayer below the phase transition, then the major part of the DPH molecules would be oriented close to the normal to the bilayer surface. It is very tempting to assign the

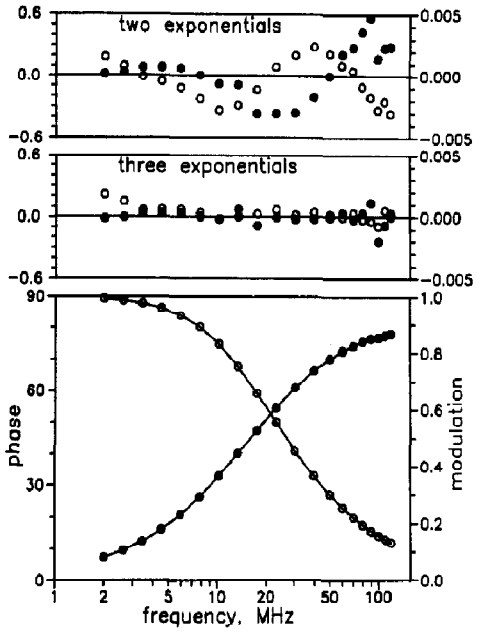

Fig. 3. Dynamic fluorescence of DPH in DPPC LUV_{100}s made in a buffer of $n_0 = 1.333$ (water); measured at 20°C. Phase: filled circles; modulation: open circles. Bottom window: experimental data and theoretical values calculated with the model of three exponentials (continuous curves). Top and central windows: zoomed deviations between experimental data and theoretical values for the models of two and three exponentials.

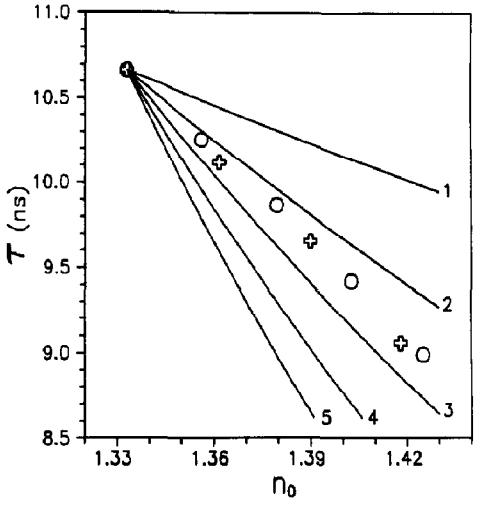

Fig. 4. The dependence of the longest lifetime component on the refractive index of the solution in which the vesicles were made. Circles and crosses represent the data obtained in the solutions of glycerol and sucrose. Curves represent negative powers of the refractive index, $\tau \sim n_0^{-m}$, the value of m being printed near each curve. The curves were normalized at the only data point that belongs to the data series obtained with both glycerol and sucrose. The total number of measurements made at this point is four times grater than at any other point. This point has also been studied by many other authors.

long lifetime component to the probe molecules oriented along the normal ($\theta = 0$), and we made such an assignment in a previous work [2]. The dependence of this lifetime component on the refractive index shown in Fig. 4 mitigates against such an assignment. The radiative decay rate of a probe oriented along the normal should change as the fifth power of the refractive index. Taking into account the value of the quantum yield, $\eta = 0.88$, we can expect that the lifetime will behave approximately like $n_0^{-4.4}$. Experimental data obtained with glycerol and sucrose fall on

Table 1

Decay of DPH in DPPC LUV_{100}s made in different solutions. C_s is the concentration of solvent, n_0 is the refractive index of the solution; τ_i and f_i are the lifetimes and intensity contributions. All data obtained at 20°C

C_s (g/l)	n_0	τ_1 (ns)	f_1 (%)	τ_2 (ns)	f_2 (%)	τ_3 (ns)	f_3 (%)
water							
–	1.333	0.1	1.0	5.9	7.7	10.66	91
glycerol							
200	1.356	0.0	0.5	5.9	7.5	10.25	92
400	1.380	0.0	0.2	5.9	8.5	9.86	91
600	1.403	0.0	0.1	5.3	7.7	9.42	92
800	1.425	0.5	0.1	5.2	8.6	8.99	91
sucrose							
200	1.362	0.1	0.4	5.2	4.4	10.12	95
400	1.390	0.2	0.2	5.3	5.9	9.65	94
600	1.418	0.3	0.1	4.6	5.0	9.06	95

one line between n_0^{-2} and n_0^{-3}. For the population parallel to the surface the lifetime would behave like n_0^{-1}. It can be concluded that the long lifetime component corresponds either to a tilted population of the probe, or to an unresolved distribution of different orientations.

The assignment of the lifetime components can be approached from a different point of view. The longest ($\theta = 0$) and the shortest ($\theta = 90°$) lifetimes of a probe in a thin film should differ by a factor of $(n_1/n_0)^4$ or less. The value of this factor is 1.3 in water and it decreases with the concentration of glycerol or sucrose. We have simulated a number of distributions where the ratio of the longest and the shortest time was 1.3, including a Gaussian distribution with chopped tails, rectangular and trapezoidal distributions. We found that all these distributions could adequately be fit by a monoexponential decay model. The worst fit was obtained in the case of a rectangular distribution, but even in this case the phase and modulation peak deviations were below 0.1° and 0.002, respectively. This suggests that at the present accuracy level it is impossible to resolve the distribution of lifetimes corresponding to different orientations, and that the lifetime τ_3 represents the average over this distribution.

The assignment of τ_2 is still unclear and although other explanations have also been proposed [16], it may have its origin in different local environments of DPH in the gel-phase membrane. The value of the constant f in Eq. (3) will depend on the local environment of the probe, so that the radiative decay rate can be different in different local environments. The value of the non-radiative rate depends on the accessibility to quenchers. Due to rapid diffusion, all probe molecules will be equally accessible to quenchers in the liquid phase. In the gel phase, however, some probe molecules may be located very close to a quencher molecule, and these will be revealed by their shorter lifetime. It is also possible that DPH may play the role of self-quencher, because the values of τ_2 and f_2 appear to depend on the concentration of DPH in lipid, As yet, however, there is insufficient evidence to support this hypothesis. The very short lifetime, present only at a minute level, almost certainly has an artifactual origin in scattered light. The samples containing sucrose have a small contamination from background fluorescence which may explain the shortening of τ_2 observed there.

4.4. Steady-state anisotropy

The physical state of the bilayer interior was monitored by measuring the value of the steady-state fluorescence anisotropy, r_{ss}, after every lifetime measurement. The values of r_{ss} obtained in all solutions except those containing sucrose fell in the range of 0.336 to 0.340. The value obtained in water was 0.338 ± 0.001. The values obtained in sucrose solutions are slightly lower, which can be due to optical activity of sucrose or background fluorescence. Even so, none of the values fell below 0.323. These experiments were carried out with samples held at 20°C, with 365 nm excitation, and a lipid concentration of 0.9×10^{-4} M. The use of higher lipid concentrations and shorter excitation wavelengths resulted in lower emission anisotropy values due to light scattering.

4.5. Orientational order

In section 2 it has been shown that, in principle the order parameter $\langle P_2 \rangle$ can be evaluated from the change in lifetime with the change in refractive index of the solution. The order parameter will be evaluated for the population of DPH that exhibits the long lifetime component. This component contributes more than 90% of fluorescence intensity, so the mean lifetime differs from the long lifetime component by less than 5%. The intermediate lifetime, τ_2 shows a similar dependence on the refractive index, however, experimental errors in its value are at least 20 times greater than in the long lifetime, preventing its use in the analysis.

Using $\eta = 0.88$ and $\tau = 8.99$ ns, determined for the $n_0 = n_1$ condition, the value of $k_{nr} = 1.33 \times 10^{-2}$ ns^{-1} was calculated from eq. (9). This value was substituted in eq. (11). Fig. 5 presents experimental data in the coordinates defined in eq. (11). The coefficients $A = 0.00871$ ns^{-1} and $B = 0.0327$ ns^{-1} were obtained by linear regres-

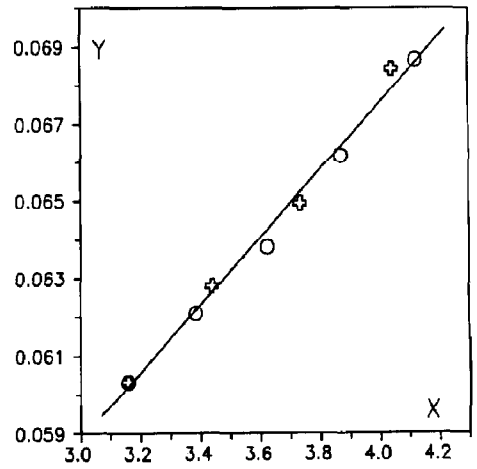

Fig. 5. Same data as in Fig. 4. plotted in the linearized coordinate system, eq. (9). Estimated $\sigma y \approx 0.0017$. The position of straight line was determined by linear regression.

sion (correlation coefficient $r^2 = 0.996$). Estimated from eq. (12), the value of $\langle P_2 \rangle$ equals 0.285 provided that $n_1 = 1.425$. Taking into account the possibility of an error in n_1, we calculated $\langle P_2 \rangle$ for a range of hypothetical values of the refractive index in the hydrocarbon region of membrane bilayer. The variation of $\langle P_2 \rangle$ between 0.176 and 0.385 resulted from the variation of n_1 between 1.325 and 1.525 (the latter range of refractive indices is much wider than that of saturated hydrocarbons).

Determination of k_{nr} using eq. (9) did not take into account the fact that the decay of DPH in membranes is double-exponential. The quantum yields of two populations of DPH associated with the lifetimes τ_2 and τ_3 can be different. It can be shown, that the quantum yield associated with the longest lifetime cannot be less than 0.87 provided that the mean quantum yield is 0.88. The reduced quantum yield results in the increased value $\langle P_2 \rangle = 0.299$, which represents the maximum possible deviation that could result from neglecting the contribution of τ_2 in our calculations.

5. Discussion

The estimation of the order parameter from the change in lifetime as a function of refractive index change involves at least two assumptions: first, the lipid suspensions obtained in all solutions were vesicles rather than micelles or thick multilayers (thicker than ≈ 50 nm), and second, the physical characteristics of the lipid bilayers, such as refractive index, etc., were independent of the chemical composition of the solution in which the vesicles were made.

As far as the first assumption is concerned, it has been shown that the extrusion technique yields calibrated size large unilamellar vesicles at least in water [13]. It is unlikely that this technique will yield micelles or extremely thick multilayers in other solutions.

The assumption that physical characteristics of the lipid bilayer and the probe–bilayer relationship are independent of the chemical composition of the solution is open to question. Scanning calorimetry data demonstrated that both the phase transition temperature of DPPC bilayers and the specific heat depend on the concentration of glycerol and other carbohydrates [17,18]. High concentrations of glycerol or sucrose shifted the phase transition temperature by ≈ 1°C. In this work all measurements were carried out at a temperature of 20°C, well below the phase transition of DPPC (41°C). At this temperature the physical characteristics of the bilayer should remain essentially constant even if the phase transition temperature shifts by 1°C. Furthermore, surface pressure studies of phospholipid monomolecular films formed at an air/water interface showed that the physical characteristics of DPPC layers below the phase transition temperature are independent of the concentration of glycerol [19]. There are NMR and EPR studies showing the effect of carbohydrates on the orientational order in phospholipid bilayers [20,21], however, these studies were made on liquid or mixed-phase bilayers. There are differing opinions regarding the effect of carbohydrates, including the suggestion that any effect observed is due to impurities [22].

In the present study, the steady-state fluorescence anisotropy was employed as an indicator of the physical characteristics of the bilayer. It is known that the value of the steady-state anisotropy changes more than five times during the phase transition, whereas fluorescence life-

time and intensity change only by some 30%. The variation of the steady-state anisotropy was less than 1% when the concentration of glycerol was varied between 0 and 800 g/l, therefore, we expect that the effect of glycerol on the physical characteristics of the bilayer interior is insignificant. In addition, the lifetimes measured in solutions containing glycerol and sucrose fall on the same line (Fig. 4), which would not be the case if either additive perturbed the physical characteristics of the bilayer interior.

In this work the value of the second-rank order parameter, $\langle P_2(\cos\theta)\rangle = 0.285$, has been estimated from the dependence of DPH lifetime on the refractive index of the medium surrounding DPPC bilayers. A second-rank order parameter which may or may not be equivalent to this can also be evaluated from time-resolved fluorescence depolarization data using [6–11]

$$r_\infty = r_0\langle P_2(\cos\theta')\rangle^2, \qquad (13)$$

where r_0 and r_∞ are the values of the time-resolved fluorescence anisotropy, $r(t)$, at the time of excitation ($t = 0$) and at the infinitely long time after the excitation ($t = \infty$); and $\langle P_2(\cos\theta')\rangle$ is this second-rank order parameter. Eq. (13) was originally derived for a uniaxial monodomain mesophase [9,10], and the angle θ' is measured from the axis of this mesophase, also known as the local director [11].

The value of r_0 for DPH is very close to 0.4 [23], while the value of r_∞ for DPH in DPPC at 20°C is greater than 0.3. This value can be obtained from our previously published data [2,3], but it can also be estimated from the value of the steady-state anisotropy [8],

$$r_\infty = r_{ss} - \frac{\phi}{\tau}(r_0 - r_{ss}), \qquad (14)$$

where ϕ and τ are the characteristic average correlation times of depolarization and fluorescence decay. Taking into account that for DPH in DPPC the ratio ϕ/τ does not exceed 1/8 and using the value of $r_{ss} = 0.338$ obtained in this work, we end up with $r_\infty \geqslant 0.330$. Substituting the latter value in eq. (13) yields $\langle P_2(\cos\theta')\rangle = 0.91$. The latter value is substantially higher than the one obtained from the lifetime dependence on the refractive index. If the value of $\langle P_2\rangle = 0.285$ was substituted in eq. (11), then the resulting value of r_∞ would be 0.032, which is a typical value obtained above rather than below the phase-transition temperature.

Several explanations of the disagreement between the values of the second-rank order parameters obtained from the variation of lifetime with refractive index and from fluorescence depolarization measurements are possible. Only a small change in refractive index is experimentally available, and the small sampling of the theoretical data surface increases the errors in our results. It is also possible that in the gel-phase membrane one does not obtain a reliable measure of r_∞ using a fluorescent probe with the lifetime in the nanosecond range. Finally, it is possible that the gel-phase membrane is not a uniaxial mesophase or that it is a uniaxial mesophase, but the orientation of the local director is not normal to the surface of the bilayer. Throughout this report θ denotes the angle measured with respect to the normal to the bilayer surface, whereas θ' denotes the angle measured with respect to the local director. If the orientation of the local director makes an angle θ'' with the normal to the bilayer surface, and the orientational distribution measured with respect to the local director is independent of the orientation of the director itself, then the following relation can be obtained using the properties of second-rank spherical tensors:

$$\langle P_2(\cos\theta)\rangle = \langle P_2(\cos\theta')\rangle\langle P_2(\cos\theta'')\rangle \qquad (15)$$

Eq. (15) yields $\langle P_2(\cos\theta'')\rangle = 0.31$. If the local director always makes the same angle with the normal, then this angle is $\theta'' = 43°$. Such a deviation of the director from the normal can be related with the tilt of DPPC acyl chains discovered in X-ray diffraction experiments [24,25].

It is also possible that the orientation of the local director is individual for every DPH molecule, which implies that DPH molecules are stranded at different orientations between the frozen acyl chains, and they can wobble within some angles, but they cannot significantly change their orientation at least on the time scale of several nanoseconds. The latter model of ran-

domly oriented "temporal" local directors is equivalent to the statement that in the gel-phase membrane one cannot measure r_∞ using a fluorescent probe with the lifetime in the nanosecond range.

The idea that the orientation of the director may not coincide with the normal to the membrane surface has not been taken into account in fluorescence depolarization studies of membranes. In the experiments with non-macroscopically orientated bilayers, reorientation of the probe rather than its absolute orientation is monitored, therefore the orientation of the director with respect to the bilayer cannot be determined. The results obtained with orientated bilayers were interpreted under an a priori assumption that the orientation of the director is normal to the bilayer surface [26]. In the theory of liquid crystals the orientation of the director is always assumed to be known, because there are a number of ways to measure it directly, including birefringence and linear dichroism. Information on the linear dichroism of DPH in bilayer membranes is not yet available and thus the question of the orientation of the director with respect to the bilayer is still open.

Acknowledgement

We thank Dr. T. Thompson, Dr. B.R. Lentz, and Dr. L. Davenport for discussing the bilayer literature related to these studies with us. We thank Dr. B. Lentz for making a review on bilayers available to us prior to publication. We thank Dr. R.E. Dale for valuable discussions and for making his results on refractive index matching available to us prior to publication.

This work is supported by NIH Grant No. GM 11632.

Appendix A

The theory for the radiative decay rate for a fluorescent probe in a thin layer (eq. (3)) is at the basis of the experiments reported here. Expressions for the radiative decay rate can be found in most textbooks on quantum electronics [27,28], but those expressions are usually derived for vacuum or for an ideal homogeneous medium, and do not take into account the difference between the local and macroscopic electromagnetic field. The difference between the local field experienced by a fluorescent probe in a thin layer and the macroscopic field outside the layer will now be considered. Lukosz [1] obtained a result similar to eq. (3) for the radiation of a classical dipole in a thin layer. Here eq. (3) is derived for a quantum object, i.e. a fluorescent molecule.

The radiative decay rate, i.e. the probability per unit time of spontaneously emitting a photon by an excited molecule, is given by

$$k_r = \frac{2\pi}{\hbar}\rho(\hbar\omega)|H'_{12}|^2, \qquad \text{(A1)}$$

where $\hbar$ is Planck's constant, $\rho(\hbar\omega)$ is the density of states of the electromagnetic field per unit energy, $\hbar\omega$ is the energy of the photon, ω is the circular frequency of light, and H'_{12}, is the matrix element of the interaction Hamiltonian corresponding to the transition between the excited state and the ground state. Since only one transition is being considered, the subscripts of the matrix element will be omitted for notation simplicity.

In unlimited space, the density of states is infinite, while the matrix element of the interaction Hamiltonian is zero. To resolve the resulting uncertainty, the system is usually placed in a finite rectangular box of dimensions $L_x \times L_y \times L_z$. If the dimensions of this box are much greater than the light wavelength, then the radiative rate will depend neither on the dimensions of the box, nor on the boundary conditions. This probability will not change when the box is removed.

The configuration of the electromagnetic field in the box depends on the boundary conditions. Cyclic boundary conditions result in a convenient expression for the field,

$$\boldsymbol{E}(\boldsymbol{r}, t) = \sum_{\boldsymbol{k}} \boldsymbol{E}_{\boldsymbol{k}} \exp(\mathrm{i}\boldsymbol{k}\cdot\boldsymbol{r} - \mathrm{i}\omega t) + \text{c.c.}, \qquad \text{(A2)}$$

where $\boldsymbol{E}(\boldsymbol{r}, t)$ is the macroscopic electric field vector, $\boldsymbol{r}$ being the radius vector, t is time, $\boldsymbol{E}_{\boldsymbol{k}}$ is

the amplitude of the field in the mode characterized by the wave vector $\boldsymbol{k}$, and c.c. stands for the complex conjugate of the preceding term. The components of the wave vector $\boldsymbol{k}$ must satisfy the cyclic conditions

$$k_x L_x = 2\pi m_x,$$
$$k_y L_y = 2\pi m_y,$$
$$k_z L_z = 2\pi m_z, \tag{A3}$$

where m_x, m_y, and m_z are integers. From eqs. (A3), the volume in the wave vector space corresponding to a single radiation mode can be determined,

$$V_k^{(1)} = 8\pi^3 / L_x L_y L_z. \tag{A4}$$

The relationship between the frequency and the wave vector is

$$\omega = \frac{c}{n_0} |\boldsymbol{k}|, \tag{A5}$$

where c is the speed of light in vacuum and c/n_0 is that in the medium of refractive index n_0. Throughout this work the subscript 0 is associated with the medium surrounding the thin layer (bilayer membrane). Rigorously speaking, eq. (A2) and subsequent equations hold only for homogeneous media. However, if the fraction of the medium with the other refractive index is very small and the light wave can travel a distance equal to the largest dimension of the box without scattering, then eq. (A2) can be still used for the macroscopic field in the predominant medium.

Using relation (A5), the volume in the wave vector space per unit energy can be determined,

$$\frac{\mathrm{d}V_k}{\mathrm{d}\hbar\omega} = \frac{4\pi\omega^2 n_0^3}{\hbar c^3}. \tag{A6}$$

Combining eqs. (A4) and (A6) and remembering that the electromagnetic wave has two polarizations, so that there are two states of the electromagnetic field per radiation mode, we obtain the density of states,

$$\rho(\hbar\omega) = \frac{\omega^2 n_0^3}{\pi^2 \hbar c^3} L_x L_y L_z. \tag{A7}$$

The amplitude of the electric field corresponding to one photon can be determined from the photon energy. The energy of the photon is equally divided between the electric field and the magnetic field, therefore the electric field carries one half of the energy,

$$\int\int\int \frac{\epsilon_0}{8\pi} |\boldsymbol{E}(\boldsymbol{r}, t)|^2 \, \mathrm{d}^3 r = \tfrac{1}{2}\hbar\omega, \tag{A8}$$

where ϵ_0 is the optical dielectric permittivity of the predominant medium. ϵ_0 should not be confused with the absolute dielectric permittivity of vacuum, which appears only in the MKS system of units, whereas here the Gaussian system of units is being employed.

Substituting $\boldsymbol{E}(\boldsymbol{r}, t)$ from eq. (A2) in eq. (A8) and integrating over the volume of the box yields

$$|\boldsymbol{E}|^2 = \frac{2\pi\hbar\omega}{\epsilon_0 L_x L_y L_z}. \tag{A9}$$

It is necessary to remember that the fluorescent probe does not interact with the macroscopic field **E**. The local field **e** experienced by the fluorescent probe can differ from the macroscopic field. However, for common amplitudes of the field, the relation between the local and macroscopic field must be linear:

$$\boldsymbol{e} = \mathbf{F}\boldsymbol{E} \tag{A10}$$

where **F** is a second-rank Cartesian tensor. The form of this tensor for the probe in the thin layer will be considered later, and first the radiative rate will be obtained for an arbitrary tensor **F**.

In the case of electric dipole transition the matrix element of the interaction Hamiltonian is

$$H' = \boldsymbol{e} \cdot \boldsymbol{\mu} \tag{A11}$$

where μ is the matrix element of the electric dipole operator. In [2,3], we introduced the apparent dipole,

$$\boldsymbol{M} = \mathbf{F}^{\mathrm{T}} \boldsymbol{\mu} \tag{A12}$$

where $\mathbf{F}^{\mathrm{T}}$ is the transposed tensor **F**. Defined in such a way the apparent dipole satisfies the relationship

$$H' = \boldsymbol{E} \cdot \boldsymbol{M}. \tag{A13}$$

The fact that the interaction between the intrinsic dipole and the local field can be formally replaced by the interaction between the apparent dipole and the macroscopic field substantially simplifies the following derivation. The states of the macroscopic field are distributed isotropically, therefore

$$|H'|^2 = \tfrac{1}{3}|\boldsymbol{E}|^2|\boldsymbol{M}|^2. \tag{A14}$$

Now eqs. (A1), (A7), (A9), and (A14) can be combined to yield

$$k_r = \frac{4\omega^3 n_0^3}{3\hbar c^3 \epsilon_0}|\boldsymbol{M}|^2. \tag{A15}$$

The magnitude of the apparent dipole involved in eq. (A15) depends on the elements of the tensor **F**. If the fluorescent probe is imbedded in a thin layer, then the tensor **F** should contain information about two sequential transformations of the field: (i) the transformation of the outside macroscopic field as it enters the thin layer and (ii) the relation between the macroscopic field inside the layer and the local field experienced by the probe. The first transformation can be conveniently described in a frame having X and Y axes parallel to the surface of the layer, and the Z axis normal to this surface,

$$E_x^{(\mathrm{in})} = E_x,$$

$$E_y^{(\mathrm{in})} = E_y,$$

$$E_z^{(\mathrm{in})} = \frac{\epsilon_0}{\epsilon_1}E_z, \tag{A16}$$

where ϵ_1 is the optical dielectric permittivity in the layer. Eqs. (A16) follow directly from the boundary conditions at the interface between two dielectrics and they correctly describe the internal macroscopic field at any point in the layer if the layer is thin compared to both the light wavelength and the radius of curvature of the surface. Eqs. (A16) are not valid for micelles and thick layers ($\lambda/8$ and thicker). In thin multilayer systems eqs. (A16) describe the field only in the layers of optical dielectric permittivity ϵ_1. The existence of intermediate layers of a different dielectric permittivity will not change the equations if the entire "sandwich" is thinner than $\lambda/8$. If the fluorescent probe is found in layers of different dielectric permittivity, e.g. both in the hydrophobic and polar regions of a phospholipid bilayer, then additional heterogeneity of the radiative decay rate is expected.

The relationship between the local and macroscopic field inside the layer is generally the same as in any other medium. H.A. Lorentz considered the relation between the local field experienced by a molecule of a medium and the macroscopic field in the medium [29] and he came to the conclusion that the two fields differ by the scalar factor

$$f = \frac{\epsilon_1 + 2}{3}. \tag{A17}$$

Lorentz obtained this result by cutting out a hollow sphere around one molecule of the medium. There were two assumptions essential for validating this procedure: (i) the molecule inside the sphere was the same as every other molecule of the medium, and (ii) the environment of this molecule had a spherical symmetry. If the fluorescence probe does not have a spherical shape, it will be unreasonable to expect that its environment will have a spherical symmetry. Beside that, the fluorescent probe is not identical to the molecules of the medium. Clearly, eq. (A17) cannot be applied to calculate the local field experienced by a fluorescent probe.

In this work it will be assumed that the local field experienced by the fluorescent probe and the macroscopic field inside the layer differ by some scalar factor f, the value of this factor being unknown. This assumption together with eqs. (A16) uniquely defines the tensor **F** and the magnitude of the apparent dipole,

$$|\boldsymbol{M}|^2 = \left(\sin^2\theta + \frac{\epsilon_0^2}{\epsilon_1^2}\cos^2\theta\right) f^2 |\boldsymbol{\mu}|^2, \tag{A18}$$

where θ is the angle between the vector $\boldsymbol{\mu}$ and the Z axis. The squared module of the apparent dipole from eq. (A18) can be substituted in eq. (A15). Using the fact that the optical dielectric

constant equals the square of the refractive index, we finally arrive at eq. (3),

$$k_r = \frac{4\omega^3}{3\hbar c^3} f^2 |\mu|^2 n_0 \left(\sin^2\theta + \frac{n_0^4}{n_1^4} \cos^2\theta \right). \qquad \text{(A19)}$$

If the above derivation was correct, then the resulting eq. (A19) must hold for vacuum also. In vacuo $n_0 = 1$, $n_1 = 1$, and $f = 1$, therefore eq. (A19) reduces to

$$k_r = \frac{4\omega^3}{3\hbar c^3} |\mu|^2. \qquad \text{(A20)}$$

The right side of eq. (A20) represents the well known expression for the Einstein coefficient A in vacuo [27].

References

1 W. Lukosz, Phys. Rev. B 22 (1980) 3030.
2 D. Toptygin, J. Svobodova, I. Konopasek and L. Brand, SPIE 1640, Time-Resolved Laser Spectroscopy in Biochemistry III (1992) 739.
3 D. Toptygin, J. Svobodova, I. Konopasek and L. Brand, J. Chem. Phys. 96 (1992) 7919.
4 E.S. Rowe, Biochim. Biophys. Acta 685 (1982) 105.
5 T. Uso and M. Rossignol, FEBS Letters 167 (1984) 69.
6 M.P. Heyn, FEBS Letters 108 (1979) 359.
7 F. Jähnig, Proc. Natl. Acad. Sci. USA 76 (1979) 6361.
8 G. Lipari and A. Szabo, Biophys. J. 30 (1980) 489.
9 C. Zannoni, Mol. Phys. 42 (1981) 1303.
10 C. Zannoni, A. Arcioni and P. Cavatorta, Chem. Phys. Lipids 32 (1983) 179.
11 A. Szabo, J. Chem. Phys. 81 (1984) 150.
12 B.R. Lentz, Chem. Phys. Lipids 64 (1993) 99–116.
13 R. Nayar, M.J. Hope and P.R. Cullis, Biochim. Biophys. Acta 986 (1989) 200.
14 R.C. Weast, ed. CRS Handbook of Chemistry and Physics (CRC Press, Boca Raton, 1987).
15 I.B. Berlman, Handbook of Fluorescent Spectra of Aromatic Molecules (Academic Press, New York, 1965).
16 T. Parasassi, G. de Stasio, R.M. Rusch and E. Gratton, Biophys. J. 59 (1991) 466.
17 R.V. McDaniel, T.J. McIntosh and S.A. Simon, Biochim. Biophys. Acta 731 (1983) 97.
18 B.Z. Chowdhry, G. Lipka and J.M. Sturtevant, Biophys. J. 46 (1984) 419.
19 J.H. Crowe, M.A. Whittam, D. Chapman and L.M. Crowe, Biochim. Biophys. Acta 769 (1984) 151.
20 K. Nicolay, E.B. Smaal and B. de Kruijff, FEBS Letters 209 (1986) 33.
21 W.K. Surewicz, Chem. Phys. Lipids 34 (1984) 363.
22 E.M. Arnett, N. Harvey, E.A. Johnson, D.S. Johnson and D. Chapman Biochemistry 25 (1986) 5239.
23 S. Kawato, K. Kinosita Jr. and A. Ikegami, Biochemistry 16 (1977) 2319.
24 J. Katsaras, D.S. Yang and R.M. Epand, Biophys. J. 63 (1992) 1170–1175.
25 S. Tristram-Nagle, R. Zhang, R.M. Suter, C.R. Worthington, W.-J. Sun and J.F. Nagle, Biophys. J.
26 R.P.H. Kooyman, M.H. Vos and Y.K. Levine, Chem. Phys. 81 (1983) 461–472.
27 W.P. Healy, Non-relativistic quantum electrodynamics (Academic Press, New York, 1982).
28 A. Yariv, Quantum Electronics (Wiley, New York, 1989).
29 H.A. Lorentz, The theory of electrons and its applications to the phenomena of light and radiant heat (Teubner, Leipzig, 1909).